Dewetting in immiscible polymer bilayer films

J. Lal,[1,2,3] S. Malkova,[2] M. K. Mukhopadhyay,[4] S. Narayanan,[1] A. Fluerasu,[5] S. B. Darling,[6] L. B. Lurio,[3] and M. Sutton[7]

[1]*X-ray Science Division, Argonne National Laboratory, Argonne, Illinois 60439, USA*

[2]*Intense Pulsed Neutron Source, Argonne National Laboratory, Argonne, Illinois 60439, USA*

[3]*Department of Physics, Northern Illinois University, DeKalb, Illinois 60115, USA*

[4]*Department of Physics, University of California, San Diego, La Jolla, California 92093-0354, USA*

[5]*NSLS-II, Brookhaven National Laboratory, Upton, New York 11973, USA*

[6]*Nanoscience and Technology Division, Argonne National Laboratory, Argonne, Illinois 60439, USA*

[7]*Physics Department, McGill University, Montréal, Canada H3A 2T8*

(Received 27 April 2016; revised manuscript received 28 November 2016; published 19 June 2017)

We have measured *in situ* the progression of dewetting from a large number of holes in immiscible polymer bilayer films. Using x-ray photon correlation spectroscopy (XPCS) in grazing incidence we probe independently the evolving dewetting process both at the top surface and the buried interface of the bilayer. At an early stage, differences in the evolution of the velocities measured by XPCS between the surface and buried interface indicate that the holes do not penetrate the bottom layer. The rim velocity at late stages decays according to a wave-vector-dependent power law, which indicates inhomogeneous flows in the film. The changes in the static scattering show that observed slow-down of the dewetting velocity is correlated with the changing roughness at the buried interface of the polymer bilayer.

DOI: 10.1103/PhysRevMaterials.1.015601

Though dewetting is a common phenomenon in nature, the mechanism governing the retreat of thin polymer films on a substrate began to be understood only recently [1–7]. De Gennes established a general theory for mobile polymer interfaces during dewetting and wetting [1,3–5]. Several works studied wetting (spreading) and dewetting using optical techniques and atomic force microscopy (AFM) [8–14]. The experiments are often not *in situ*; they mostly probe the surface topography and provide the dewetting velocity of rims around a single hole indirectly. Further, the current theoretical models are unable to capture the range of competing effects in dewetting kinetics in polymer thin films. A comprehensive statistical picture of dewetting via heterogeneous nucleation does not exist. For example, AFM is unable to probe how nucleation of new holes may affect the dynamics of existing holes, since only one hole can be followed at a time.

So far, most studies explored the dewetting of single-layer polymer films on solid substrates, where it is sufficient to study the unstable top polymer surface [15]. The more complex dewetting in a polymer bilayer, where the top polymer layer dewets from a deformable polymer underlayer, has received less attention [10–13]. Polymer-on-polymer dewetting presents an experimental challenge since one of the interfaces is buried. Insight from these studies sheds light on the interfacial phenomena of wetting, adhesion, and friction in thin polymer films, where mobile borders are involved. The present *in situ* study focuses on dewetting initiated by nucleation of holes in supported viscoelastic bilayer films.

Previous work on single holes [1] has shown that capillarity represents the main driving force for spreading or dewetting. The dewetting is opposed by viscous or viscoelastic dissipation within the polymer film and frictional losses at the substrate. When the increase in dewetting driving force is smaller than the increase in frictional force, the fluid starts to collect in a "rim" close to the moving three-phase contact line [9].

A full statistical picture of the temporal evolution of dewetting is difficult to obtain by optical microscopy and AFM, while for x rays large-scale, multiple-hole dynamics is the natural probe mechanism. There have been attempts to probe spreading of droplets and dewetting in films using x-ray scattering [15–17]. X-ray photon correlation spectroscopy (XPCS) is a unique experimental method enabled by high-brightness third-generation synchrotron sources ideally suited to measure mesoscale dynamics in condensed-matter systems [18,19]. In the present work, two-time correlation functions (TTCFs) [19] measured by XPCS in grazing incidence provide *in situ* snapshots of the dewetting process, particularly the dewetting velocity at the top and buried interface.

The system studied was a poly(4-bromo styrene) (PBrS) thin film deposited on an immiscible and nonwettable polystyrene (PS) sublayer on a silicon substrate. Monodisperse PS (molecular weight $M_w = 207$ kDa from Pressure Chemical) and PBrS ($M_w = 350$ kDa, the fraction of brominated monomers was 0.89) were used in these experiments. The bilayers were prepared by spin coating PBrS layers of thickness 1000 Å, 700 Å, and 400 Å onto a glass slide and then floating from de-ionized water onto the 1000 Å PS sublayer, which was previously deposited on pre-cleaned 15×15 mm silicon wafers. Viscous polymers (PBrS/PS bilayers) with high-molecular weight and thick films (∼1000 Å) were chosen to slow down the kinetic processes and enable *in situ* studies [13]. For these thick films, the holes were on average separated by several microns.

The PBrS/PS bilayers are metastable and, if heated above the glass transition [21], the top surface dewets from the PS-coated substrate. This agrees with previous PEEM measurements [20] on PBrS/PS bilayers, which showed that the diffusion and flow parallel to the interfaces is faster for both PS and PBrS than the diffusion of PS perpendicular to the PS/PBrS interface. Thus the bottom layer (PS) does not dewet at the same time as the top layer [20].

Optical images indicate [21] heterogeneous nucleation which can be due to nonequilibrated conformational states, residual stresses, and other chemical or physical

inhomogeneities [6,22]. The radial size of the holes measured by AFM varied between 8–14 μm (depending on the annealing time and on the particular hole). The AFM data [21] show a clear rim after 12 hours formed from the material collected from the hole. Symmetric rims are observed around small young holes ($\sim$10 μm) and asymmetric rims are found around large mature holes ($\sim$30 μm) irrespective of the thickness of the top bilayer. We believe that the rims are the primary source of scattering contrast in the dewetting process.

Grazing-incidence XPCS experiments were performed at energy of 7.35 keV with beamsize 20 μm at the sector 8-ID-I beamline at the Advanced Photon Source, Argonne National Laboratory. The samples were held at 170 °C, above the glass transition [21] of the polymers, and the evolving off-specular diffuse scattering was monitored as a function of annealing time using a charge-coupled device (CCD) detector with 22 μm pixels located 4.8 m downstream of the sample. Each frame was recorded with an exposure time of 0.2 s and a time interval between successive frames of 8.32 s. The zero of the waiting time t_w corresponded to the initial temperature quench from 150 °C (where it pre-annealed $\sim$2 hours during sample alignment) to 170 °C. XPCS data was collected until late in the dewetting process ($t_w \sim 7$ hours) in 1.2 hours time steps, alternating between measurements of the dynamics at the top surface and the buried interface. For x rays incident at an angle ($\theta_{in} = 0.175°$) smaller than the critical angle of the top layer ($\alpha_c = 0.191°$ for PBrS), all of the scattering originates from the top layer. Following a reverse standing-wave method described in Refs. [23,24], a larger incident angle was chosen ($\theta_{in} = 0.225°$) to yield scattering dominated by the buried interface of the bilayer [21]. For $\theta_{in} = 0.175°$ the footprint of the x-ray beam was approximately 7 mm so that around 250 holes were illuminated (assuming an average hole size of 10 μm and spacing between holes $\sim$20 μm).

The nonstationary dynamics associated with the out-of-equilibrium dewetting process were measured by means of TTCFs (Fig. 1) [25],

$$C(q,t_1,t_2) = \frac{\langle I(q,t_1)I(q,t_2)\rangle}{\langle I(q,t_1)\rangle\langle I(q,t_2)\rangle}. \quad (1)$$

Examples of TTCFs averaged over a region of pixels with the same in-plane component of the scattering wave vector $q_\parallel \sim 2.78 \times 10^{-4}$ Å^{-1} are shown in Figs. 1(a)–1(f). The natural variables describing TTCFs are the "dewetting time" $t_a = (t_1 + t_2)/2$, measured along the $t_1 = t_2$ diagonal and the time difference $t = |t_1 - t_2|$ corresponding to the distance from the same diagonal. The "one-time" slices $t_a = \text{const}$ [dotted line in Fig. 1(e)] are fitted based on Eq. (3) below (solid lines), and nonstationary effects can be observed by fitting successive slices representing $g^{(2)}(q_\parallel t) - 1$ [Fig. 1(h)].

Assuming that the dewetting ring can be modeled by a rim velocity that is slowly varying so that the change in structure (within $t_a = 1.2$ hours) can be ignored, a variant of Fuller's model [26] can be used to describe the data, yielding the normalized intermediate scattering function $g^{(1)}(q_\parallel t)$ in terms of a Bessel function J_0. Using $q_\parallel$ and the in-plane velocity V_0 of the rims associated with the dewetting process, $g^{(1)}(q_\parallel t)$ can

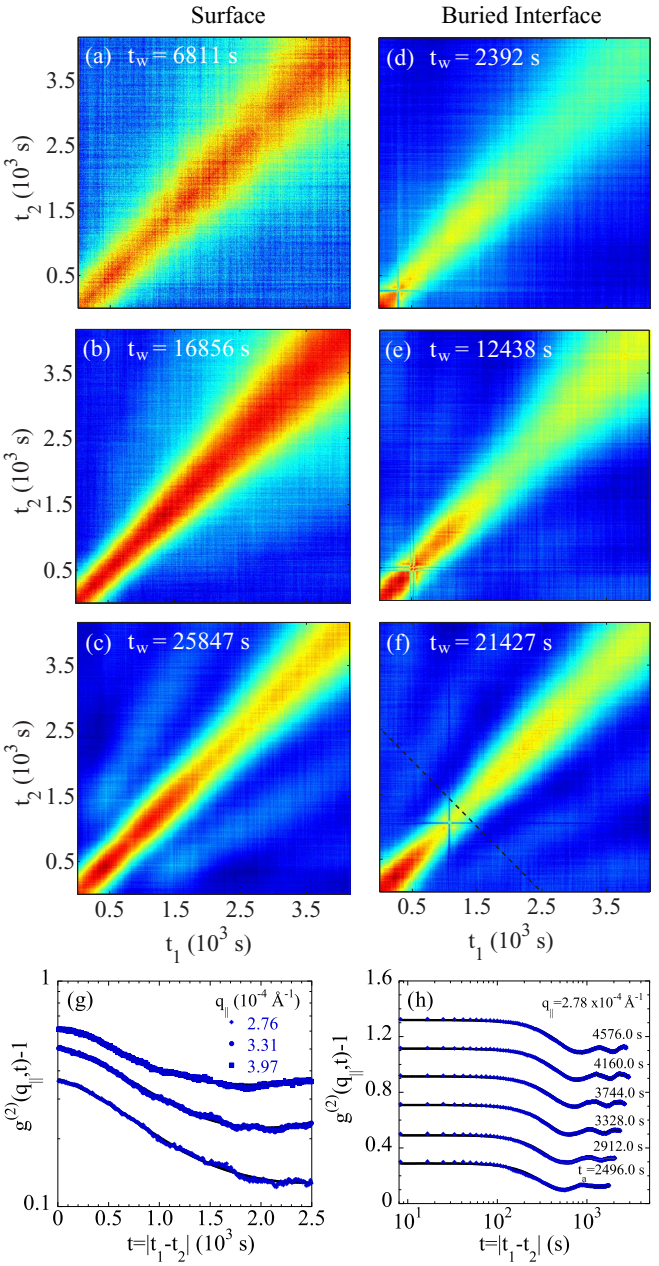

FIG. 1. TTCFs measured from the top surface and buried interface of the bilayer at $q_\parallel \sim 2.78 \times 10^{-4}$ Å^{-1}. The t_w for the measured TTCFs are (a) 6811 s, (b) 16856 s, (c) 25847 s, and (d) 2392 s, (e) 12438 s, (f) 21427 s, respectively. $g^{(2)}(q_\parallel t) - 1$ for the buried interface (g) at $t_a = 4576$ s and $t_w = 2392$ s and (h) $t_w = 21427$ s as a function of $t = |t_1 - t_2|$. Solid lines in (g) and (h) are fits based on Eq. (3). For clarity, the curves in panel (h) starting with the second one were shifted up in multiples of 0.2.

be expressed as [21]

$$g^{(1)}(q_\parallel t) = \frac{1}{2\pi}\int_0^{2\pi} e^{i\sqrt{A^2+B^2}\sin(\phi+\psi)}d\phi = J_0(q_\parallel V_0 t). \quad (2)$$

This is related to the intensity autocorrelation function $g_2(q_\parallel t)$ via the Siegert relationship, $g_2(q_\parallel t) = 1 + \beta|g_1(q_\parallel t)|^2$, where A, B, and ψ are defined in the Supplemental Material [21] and

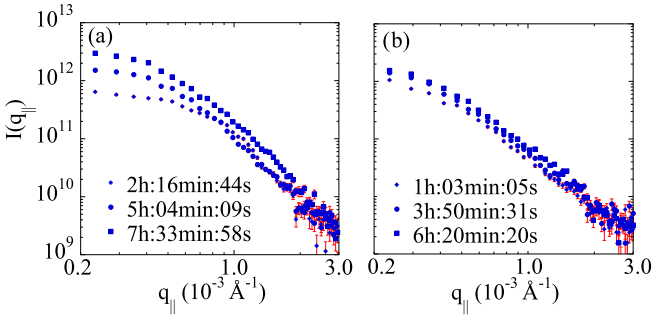

FIG. 2. Average static diffuse scattering from (a) surface and (b) buried interface of the bilayer corresponding to TTCFs in Figs. 1(b), 1(c), 1(e), and 1(f).

β is the optical contrast. Thus,

$$g^{(2)}(q_\parallel t) = \beta J_0^2(V_0 q_\parallel t) + 1. \quad (3)$$

The characteristic oscillations reflecting the asymptotic form of $J_0 \sim \sin(q_\parallel V_0 t)/(q_\parallel V_0 t)$ can be clearly seen for the time slices in Fig. 1(h), thus demonstrating the validity of the model described in Eq. (3).

To take account of polydispersity in the sizes of holes (thus, the rims around them) indicated by optical micrographs [21], a Gaussian distribution of velocities $P(v) = \frac{1}{\sigma\sqrt{2\pi}} e^{-(V_0-V)^2/2\sigma^2}$ was assumed with mean velocity V and variance σ. The Gaussian was convoluted with the Bessel function, and a numerical integration was performed at each time step for successive slices of $g^{(2)}(q_\parallel t) - 1$ to get the mean velocity V. The variance σ reflects the average distribution of velocities within rims of different sizes hence samples an average rim size [21].

The time average "static" diffuse scattering from the top surface corresponding to Figs. 1(b) and 1(c) is shown in Fig. 2(a) and that corresponding to the buried interface Figs. 1(e) and 1(f) is shown in Fig. 2(b). After five hours, a large change of static diffuse intensity is observed from the top surface, which indicates that a significant number of rims around holes have formed. Meanwhile, the static diffuse intensity from the buried interface shows very small increases at low $q_\parallel$ during this time [Fig. 2(b)] which implies that the interface tension slightly decreases [23,27]. The latter can be related to the very small interdiffusion between the immiscible PS and PBrS polymer chains (on a segmental level) and interface roughening due to capillary waves. This small increasing roughness of the buried PS/PBrS interface is estimated to be between 20 Å at early times and more than 26 Å for longer times [21]. This implies the contribution from friction (k) is increasing and slip length (b) is decreasing [28] with increasing roughness at the buried interface. The slip length is $b = \eta/k$, where η is the polymer viscosity. It has been shown that a decrease of b with increasing k induces a decrease of the maximum rim width $w = \sqrt{bh}$, where h is the thickness of the film [29–31]. Thus decreasing slip lengths can lead to decreasing widths of rims leading to asymmetric rim profiles [21,32].

Figure 3 shows the mean velocities V for $q_\parallel \sim 2.78 \times 10^{-4}$ Å^{-1} as a function of t_a and for increasing values of t_w resulting from fits based on Eq. (3). Data for the top surface

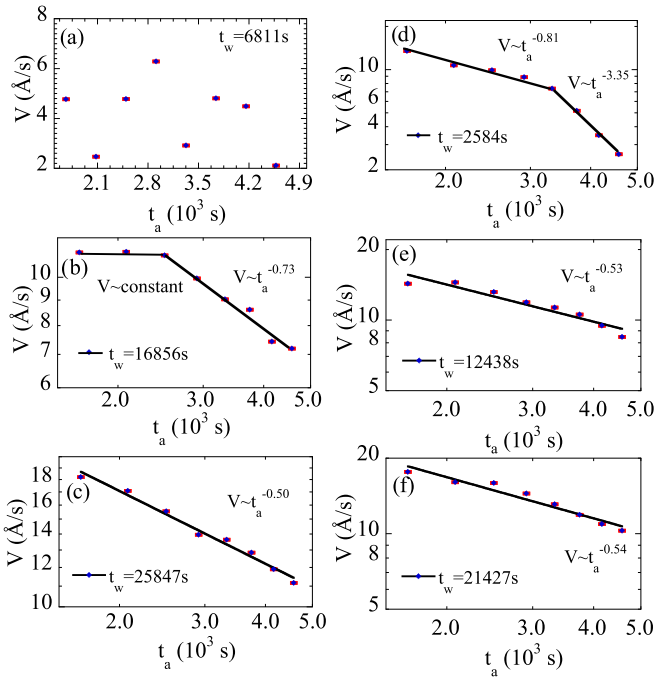

FIG. 3. Mean velocities V as a function of t_a for increasing values of t_w. Results for the top surface are shown in panels (a)–(c) and from the buried interface in panels (d)–(f) for $q_\parallel \sim 2.78 \times 10^{-4}$ Å^{-1}.

[Figs. 3(a)–3(c)] and the buried interface [Figs. 3(d)–3(f)] correspond to the TTCFs in Figs. 1(a)–1(f). The estimated error in V is extremely small. The data suggests that a large number of holes form very early ($\lesssim$1 hour) and that later times are dominated by scattering from the rims of these holes and not from capillary waves as has been seen in other polymer systems [24], except in the very beginning $t_w = 2392$ s at the buried interface [Fig. 3(d)], where $V \sim t_a^{-3.35}$ is associated with interface broadening due to capillary waves [1,23]. Initial XPCS measurements probe a regime where there are many holes opening and dynamics are chaotic, due to a superposition of mature and immature holes [Fig. 3(a)]. Later measurements ($\gtrsim$3 hours) show a more stable regime characteristic of hole growth. However, differences in scattering between the top interface and the buried interface of the bilayer indicate that most holes have not fully penetrated down to the substrate, and thus appear significantly different depending on which height in the sample is probed. Different areas of the sample may also have holes that initiated at different absolute times. Translation to different parts of the sample, in order to minimize x-ray damage, changes the hole distribution and may catch holes at different states in their time evolution (Fig. 3).

We note that the order of magnitude of the velocity V (Fig. 3) can be estimated as follows. In most capillary phenomena in the viscous regimes [1], the characteristic velocity varies as $V^* = \gamma/\eta$. Here γ is the effective interface tension between PS and PBrS [15,21] and η is the average viscosity of PS and PBrS, yielding $V^* \sim 7.29$ Å/s.

The results in Fig. 3 conform to the general behavior seen in dewetting dynamics [14,31]. As the hole opens, the whole film is elastically deformed by the capillary forces S acting at the hole periphery. The small-amplitude oscillations in Fig. 1(g)

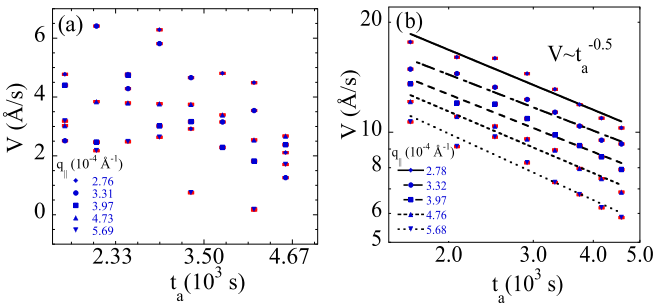

FIG. 4. Mean velocity V as a function of t_a for different wave vectors $q_\parallel$ for (a) 1000 Å top surface at $t_w = 6811$ s and (b) buried interface of the bilayer at $t_w = 21\,427$ s.

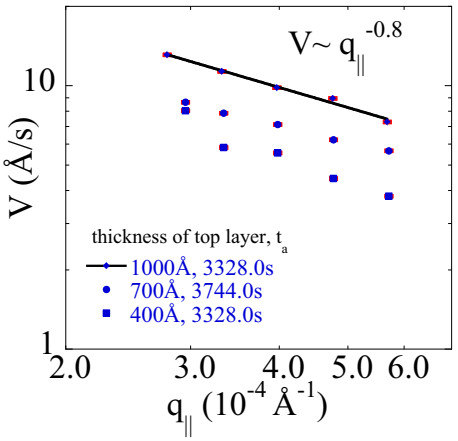

FIG. 5. Mean velocity V at the buried interface as a function of $q_\parallel$ for the t_a indicated. The t_w for the 1000 Å top layer is 21 427 s, for the 700 Å is 24 113 s and for the 400 Å is 15 364 s.

and Ref. [21] with 300 s period, which are not captured by Eq. (3), may correspond to a higher initial hole opening velocity ~60 Å/s. During the early stages the dewetted hole size increases and rim formation takes place [Fig. 2(a)], up to $V \simeq$ const [Fig. 3(b)] which identifies that we have statistically significant numbers of young rims formed. This is followed by a power law $V \sim t_a^{-0.73}$. At still later times $t_w = 25\,847$ s, $V \sim t_a^{-0.50}$ was observed [Fig. 3(c)]. The velocity decrease with increasing time reflects the nonlinear friction at the interface of PBrS/PS (see Fig. 2(b) and Ref. [21]). A small effect of residual stresses may be present in the film at early times [6,33,34]. However, due to pre-annealing at 150 °C and based on estimates of the reptation times of the polymers we expect that most stresses have relaxed [21]. Similar power law behavior $V \sim t_a^{-\alpha}$, where α is between 0.5 and 1.0, is seen for the bottom interface [Figs. 3(d)–3(f)].

Figure 4 shows the velocity as a function of t_a for different values of $q_\parallel$. Figures 3(a) and 4(a) show a randomly varying velocity as a function of t_a at the top surface of the 1000 Å film at the earliest time. This evolves towards a $q_\parallel$ dependent power law decay at later times as shown for the top interface in Fig. 3(c) and for the buried interface in Fig. 4(b). The $q_\parallel$ dependent velocity indicates inhomogeneous flows in the film. These results further indicate that wider younger rims move faster and scatter at low $q_\parallel$, whereas more mature slower rims, which are smaller in width [21], scatter at larger $q_\parallel$. This may indicate that the velocity of the rims is affected by nonlinear friction at the interface as the rim widths decrease with dewetting time. As shown in other experiments [35] this $q_\parallel$ dependence can be more complicated as holes that nucleate later are smaller in size and grow at a much smaller rate (i.e., have smaller rims and slower velocities). The $q_\parallel$ dependence of rim velocities found here thus reflects the heterogeneity of the nucleation process [21].

The $q_\parallel$ dependence $V \sim {q_\parallel}^{0.8}$ is seen for all film thicknesses h (Fig. 5). The data also shows that V decreases with decreasing h. An explanation for this behavior is that in the beginning the dewetting rates are markedly higher for thinner films [9]. Decreasing thicknesses thus show the dewetting history at later times. This implies that at the buried interface the 400 Å and 700 Å top layers have a larger contribution from the more mature rims (with smaller V) than the 1000 Å layer.

In conclusion, *in situ* snapshots of the diffuse scattering at the top and buried interface of immiscible polymer bilayer films provide a detailed probe of dewetting through the evolution of the rim velocities obtained from TTCFs. The $q_\parallel$ dependent velocities observed here indicate inhomogeneous flows in the film. As the holes get bigger, more material piles up at the rim [9], thus requiring the velocity to slow down. This is correlated to changes in the static diffuse scattering which point to the important role played by interface evolution and hence friction (suppressing slippage) in defining the asymmetric rim shapes [21,30]. The power laws observed here at late times for the average velocity are similar to those observed in AFM studies of single dewetting holes in viscoelastic polymer films deposited on a very thin polymer cushion layer on silicon substrates [6,34]. Previously it was found that merely a slip-boundary condition at the polymer-solid interface can lead to an asymmetric rim profile [32]. Our work shows that the roughness and its evolution (hence friction) at the polymer-on-polymer interface of bilayers [21,24] and similar engineered interfaces [6,29,32,34] is the most important condition for the similar dewetting kinetics of rims observed in viscoelastic thin polymer films.

This research used resources of the Advanced Photon Source and the Center for Nanoscale Materials, US Department of Energy (DOE) Office of Science User Facilities operated for the DOE Office of Science by Argonne National Laboratory under Contract No. DE-AC02-06CH11357.

[1] P. G. de Gennes, F. Brochard-Wyart, and D. Quere, *Capillarity and Wetting Phenomena: Drops, Bubbles, Pearls, Waves* (Springer, New York, 2004).
[2] S. Chandran and G. Reiter, Phys. Rev. Lett. **116**, 088301 (2016).
[3] M. E. R. Shanahan, J. Phys. D: Appl. Phys. **21**, 981 (1988).
[4] P. G. de Gennes, Rev. Mod. Phys. **57**, 827 (1985).
[5] F. Brochard-Wyart, P. Martin, and C. Redon, Langmuir **9**, 3682 (1993).

[6] G. Reiter, M. Hamieh, P. Damman, S. Sclavons, S. Gabriele, T. Vilmin, and E. Raphael, Nat. Mater. **4**, 754 (2005).
[7] P. Damman, S. Gabriele, S. Coppée, S. Desprez, D. Villers, T. Vilmin, E. Raphaël, M. Hamieh, S. Al Akhrass, and G. Reiter, Phys. Rev. Lett. **99**, 036101 (2007).
[8] F. Heslot, N. Fraysse, and A. M. Cazabat, Nature (London) **338**, 640 (1989).
[9] G. Reiter, Adv. Polym. Sci. **252**, 29 (2013).
[10] P. Lambooy, K. C. Phelan, O. Haugg, and G. Krausch, Phys. Rev. Lett. **76**, 1110 (1996).
[11] K. Kostourou, D. Peschka, A. Münch, B. Wagner, S. Herminghaus, and R. Seemann, Chem. Eng. Process. **50**, 531 (2011).
[12] R. A. Segalman and P. F. Green, Macromolecules **32**, 801 (1999).
[13] D. Slep, J. Asselta, M. H. Rafailovich, J. Sokolov, D. A. Winesett, A. P. Smith, H. Ade, and S. Anders, Langmuir **16**, 2369 (2000).
[14] G. Reiter, Phys. Rev. Lett. **87**, 186101 (2001).
[15] M. Sferrazza, M. Heppenstall-Butler, R. Cubitt, D. Bucknall, J. Webster, and R. A. L. Jones, Phys. Rev. Lett. **81**, 5173 (1998).
[16] J. Daillant, J. Benattar, L. Bosio, and L. Leger, Europhys. Lett. **6**, 431 (1988).
[17] P. Müller-Buschbaum, P. Vanhoorne, V. Scheumann, and M. Stamm, Europhys. Lett. **40**, 655 (1997).
[18] G. Grübel, A. Madsen, and A. Robert, in *Soft Matter Characterization*, edited by R. Borsali and R. Pecora (Springer, New York, 2008), pp. 953–995.
[19] M. Sutton, in *Third Generation Hard X-Ray Synchrotron Radiation Sources*, edited by D. Mills (Wiley, New York, 2002).
[20] H. Ade, D. A. Winesett, A. P. Smith, S. Anders, T. Stammler, C. Heske, M. H. Rafailovich, J. Sokolov, and J. Stöhr, Appl. Phys. Lett. **73**, 3775 (1998).
[21] See Supplemental Material at http://link.aps.org/supplemental/10.1103/PhysRevMaterials.1.015601 for derivation of the intensity autocorrelation function $g^{(2)}(q_\parallel t)$, optical and AFM images, *in situ* x-ray reflectivity curves showing the evolution of surface and interface roughness, and additional supplementary discussion with figures.
[22] K. Jacobs, R. Seemann, and S. Herminghaus, in *Polymer Thin Films*, edited by O. K. C. Tsui and T. P. Russell (World Scientific, New Jersey, London, Singapore, 2008), pp. 243–266.
[23] X. Hu, X. Jiao, S. Narayanan, Z. Jiang, S. K. Sinha, L. B. Lurio, and J. Lal, Eur. Phys. J. E **17**, 353 (2005).
[24] X. Hu, Z. Jiang, S. Narayanan, X. Jiao, A. R. Sandy, S. K. Sinha, L. B. Lurio, and J. Lal, Phys. Rev. E **74**, 010602 (2006).
[25] M. Sutton, K. Laaziri, F. Livet, and F. Bley, Opt. Express **11**, 2268 (2003).
[26] G. G. Fuller, J. M. Rallison, R. L. Schmidt, and L. G. Leal, J. Fluid Mech. **100**, 555 (1980).
[27] L. Lurio, H. Kim, A. Rühm, J. Basu, J. Lal, S. K. Sinha, and S. G. J. Mochrie, Macromolecules **36**, 5704 (2003).
[28] F. Brochard-Wyart, P. G. de Gennes, and S. M. Troian, C. R. Acad. Sci. Paris, Ser. II **310**, 1169 (1990).
[29] S. Coppee, S. Gabriele, A. M. Jonas, J. Jestin, and P. Damman, Soft Matter **7**, 9951 (2011).
[30] F. Ziebert and E. Raphael, Europhys. Lett. **86**, 46001 (2009).
[31] F. Brochard-Wyart, G. Debregeas, R. Fondecave, and P. Martin, Macromolecules **30**, 1211 (1997).
[32] O. Bäumchen, R. Fetzer, and K. Jacobs, Phys. Rev. Lett. **103**, 247801 (2009).
[33] T. Vilmin and E. Raphael, Europhys. Lett. **72**, 781 (2005).
[34] P. Damman, N. Baudelet, and G. Reiter, Phys. Rev. Lett. **91**, 216101 (2003).
[35] A. Raegen, M. Chowdhury, C. Calers, A. Schmatulla, U. Steiner, and G. Reiter, Phys. Rev. Lett. **105**, 227801 (2010).